J. Plasma Physics: page 1 of 25.
doi:10.1017/S0022377806004624

Energy transfer in Hall-MHD turbulence: cascades, backscatter, and dynamo action

PABLO D. MININNI, ALEXANDROS ALEXAKIS
and ANNICK POUQUET
National Center for Atmospheric Research, PO Box 3000,
Boulder, CO 80307, USA
(mininni@ucar.edu, alexakis@ucar.edu, pouquet@ucar.edu)

(Received 30 January 2006)

Abstract. Scale interactions in Hall magnetohydrodynamics (MHDs) are studied using both the mean field theory derivation of transport coefficients, and direct numerical simulations in three space dimensions. In the magnetically dominated regime, the eddy resistivity is found to be negative definite, leading to large-scale instabilities. A direct cascade of the total energy is observed, although as the amplitude of the Hall effect is increased, backscatter of magnetic energy to large scales is found, a feature not present in MHD flows. The coupling between the magnetic and velocity fields is different than in the MHD case, and backscatter of energy from small-scale magnetic fields to large-scale flows is also observed. For the magnetic helicity, a strong quenching of its transfer is found. We also discuss non-helical magnetically forced Hall-MHD simulations where growth of a large-scale magnetic field is observed.

1. Introduction

The relevance of two fluid effects has recently been pointed out in several studies of astrophysical and laboratory plasmas (Balbus and Terquem 2001; Sano and Stone 2002; Mirnov et al. 2003; Ding et al. 2004). The effect of adding the Hall current to the dynamics of the flow was studied in several scenarios, particularly dynamo action (Helmis 1968; Galanti et al. 1995; Mininni et al. 2002, 2003a, 2005b) and reconnection (Birn et al. 2001; Shay et al. 2001; Wang et al. 2001; Morales et al. 2005). Several of these works showed that the Hall currents increase the reconnection rate of magnetic field lines. However, most of the studies of magnetic reconnection were done for particular configurations of current sheets. It was shown, in particular by Smith et al. (2004), that when a turbulent background is present the reconnection rate is dominated by the amplitude of the turbulent fluctuations. The process of magnetic reconnection is relevant in several astrophysical and geophysical scenarios, such as the magnetopause, the magnetotail, the Solar atmosphere, or the interplanetary and interstellar medium. Reconnection can also play a role in the generation of large-scale magnetic fields by dynamo action (Zeldovich et al. 1983).

Some of the works in Hall magnetohydrodynamics (MHDs) present conflicting results, indicating in some cases that the Hall effect can help the growth of a large-scale magnetic field (Mininni et al. 2005b) or a large-scale self-organization process (Mahajan and Yoshida 1998; Numata et al. 2004; Ohsaki 2005), while in other cases

the Hall currents were observed to generate small scales and filamentation (Laveder et al. 2002a,b; Rheinhardt and Geppert 2002).

As a result, it becomes of interest to study the physical processes leading to cascades and the transfer of ideal invariants in three-dimensional Hall-MHD turbulence. Phenomena observed in the laboratory and space plasmas tend to show an intermittent or impulsive behavior (Bhattacharjee et al. 1999) characteristic of turbulent flows. The relevance of Hall-MHD turbulence in the Solar wind was shown by Ghosh et al. (1996). Also, Hall-MHD turbulence can play a crucial role in the transfer of matter in the magnetopause as was pointed by Rezeau and Belmont (2001).

In this work, we study both analytically and numerically three-dimensional Hall-MHD turbulence as the result of a dynamo process, and from a purely electromotive forcing. Detailed studies of shell-to-shell energy transfer from direct numerical simulations (DNSs) have been done for hydrodynamic (Domaradzki and Rogallo 1990; Ohkitani and Kida 1992; Zhou 1993; Yeung et al. 1995; Alexakis et al. 2005a) and magnetohydrodynamic flows (Debliquy et al. 2005; Alexakis et al. 2005b; Mininni et al. 2005a). To the best of our knowledge, the energy transfer in Hall-MHD turbulence has not been studied before.

We show evidence of non-locality of the transfer in Fourier space, and that the Hall effect can increase both the transfer of magnetic energy to smaller scales (locally), as well as give a novel non-local backscatter of magnetic energy to large scales. These results become clear when examining the modification to the turbulent magnetic diffusivity due to the Hall term. Also, we observe that the Hall currents have an impact on the coupling between the magnetic and velocity fields. The transfer of energy between these two fields is different than in the MHD case. The Hall-MHD equations also display a backscatter of energy from small-scale magnetic fluctuations to the large-scale flows themselves. The transfer of helicity is briefly discussed as well and observed to be quenched by the Hall effect.

The structure of the paper is as follows. In Sec. 2 we introduce the Hall-MHD equations and we define the various transfer terms. In Sec. 3 we derive turbulent transport coefficients for the Hall-MHD induction equation. In Sec. 4 we briefly discuss the code and details of the mechanically forced numerical simulations for completeness. Section 5 presents the transfer terms in Hall MHDs as obtained from the numerical simulations. Section 6 shows backscatter of magnetic energy in non-helical Hall-MHD magnetically forced simulations. Finally, Sec. 7 summarizes the results and discusses implications of our work for the understanding of turbulence, dynamo action, and reconnection in Hall MHDs.

2. The Hall-MHD equations and transfer terms

In dimensionless Alfvénic units, the Hall-MHD equations are

$$\partial_t \mathbf{U} + \mathbf{U}\cdot\nabla\mathbf{U} = -\nabla\mathscr{P} + \mathbf{B}\cdot\nabla\mathbf{B} + \nu\nabla^2\mathbf{U} + \mathbf{f}, \tag{2.1}$$

$$\partial_t \mathbf{B} = \nabla\times[(\mathbf{U} - \epsilon\mathbf{J})\times\mathbf{B}] + \eta\nabla^2\mathbf{B}, \tag{2.2}$$

where $\mathbf{U}$ is the bulk velocity field, $\mathbf{B}$ is the magnetic field, $\mathbf{J} = \nabla\times\mathbf{B}$ is the current density, $\mathscr{P}$ is the pressure, ν is the kinematic viscosity, and η is the magnetic diffusivity. From the Maxwell equations and incompressibility of the flow, $\nabla\cdot\mathbf{U} = \nabla\cdot\mathbf{B} = 0$.

The Hall term $\epsilon \mathbf{J} \times \mathbf{B}$ in (2.2) measures the velocity difference between species, where the electron velocity is $\mathbf{U}^{\mathrm{e}} = \mathbf{U} - \epsilon \mathbf{J}$. Here, ϵ measures the relative strength of the Hall effect, with the Hall term being dominant for wavenumbers larger than $k_{\mathrm{Hall}} \sim 1/\epsilon$ if equipartition between the fields is assumed. The measure of strength of the Hall effect can be written as $\epsilon = L_{\mathrm{Hall}}/L_0$ where L_0 is a characteristic length (we will use $L_0 = 2\pi$, the size of the box in our simulations). In terms of physical parameters, and for a fully ionized plasma, the Hall length is $L_{\mathrm{Hall}} = cU_{\mathrm{A}}/(\omega_{\mathrm{pi}} U_0)$, where U_{A} is the Alfvénic speed, U_0 is a characteristic speed, c is the speed of light, and ω_{pi} is the ion plasma frequency (when $U_0 = U_{\mathrm{A}}$, L_{Hall} reduces to the ion skin depth). In a partially ionized plasma, expressions for L_{Hall} can be found in Sano and Stone (2002) and Mininni et al. (2003a).

Of special interest is the ratio between the integral length L, the Hall length L_{Hall}, and the Ohmic dissipation length L_η. For $L_{\mathrm{Hall}} \ll L_\eta$ ($\epsilon \to 0$), the Hall-MHD equations reduce to the well-known MHD case. In several astrophysical problems, such as accretion disks, protoplanetary disks, or the magnetopause (see, e.g. Birn et al. 2001; Balbus and Terquem 2001; Sano and Stone 2002), the Hall scale is larger than Ohmic scales although smaller than the integral scale L of the flow. We will be interested in this regime in this work, although we remark that the separation between these scales in astrophysical or geophysical problems is far from what can be achieved in numerical simulations.

The Hall-MHD equations have three ideal invariants (Turner 1986). In this work we will focus on two invariants, the total energy

$$E = \frac{1}{2} \int (U^2 + B^2)\, d\mathbf{x}^3, \tag{2.3}$$

and the magnetic helicity

$$H = \frac{1}{2} \int \mathbf{A} \cdot \mathbf{B}\, d\mathbf{x}^3, \tag{2.4}$$

where $\mathbf{A}$ is the vector potential, $\nabla \times \mathbf{A} = \mathbf{B}$. These quantities are also ideal invariants of the MHD equations ($\epsilon = 0$). The third MHD invariant, the cross helicity, is replaced in Hall MHDs by the hybrid helicity (Turner 1986) and is small in the simulations we will discuss.

The expressions we will use for the shell-to-shell energy transfers have been derived for the MHD case by Verma (2004), Debliquy et al. (2005), and Alexakis et al. (2005b). Here we present the derivation of the transfer terms for the Hall-MHD equations. Equation (2.2) can be rewritten as

$$\partial_t \mathbf{B} + \mathbf{U} \cdot \nabla \mathbf{B} = \mathbf{B} \cdot \nabla \mathbf{U} - \epsilon \nabla \times (\mathbf{J} \times \mathbf{B}) + \eta \nabla^2 \mathbf{B}. \tag{2.5}$$

We introduce a filter in shells in Fourier space, such as $\mathbf{F}_K$ which denotes the components of the field with wavenumbers between K and $K+1$ (i.e. $\mathbf{F}_K(\mathbf{x}) = \sum_{k=K}^{K+1} \hat{\mathbf{F}}(\mathbf{k}) e^{i\mathbf{k}\cdot\mathbf{x}}$), from (2.1) and (2.5) we can write detailed balance equations for the energy,

$$\partial_t E_U(K) = \int \left\{ \sum_Q [-\mathbf{U}_K \cdot (\mathbf{U} \cdot \nabla) \cdot \mathbf{U}_Q + \mathbf{U}_K \cdot (\mathbf{B} \cdot \nabla) \cdot \mathbf{B}_Q] - \nu \nabla^2 \mathbf{U}_K + \mathbf{f} \cdot \mathbf{U}_K \right\} d\mathbf{x}^3, \tag{2.6}$$

$$\partial_t E_B(K) = \int \Big\{ \sum_Q [-\mathbf{B}_K \cdot (\mathbf{U}\cdot\nabla)\cdot \mathbf{B}_Q + \mathbf{B}_K \cdot (\mathbf{B}\cdot\nabla)\cdot \mathbf{U}_Q + \epsilon \mathbf{J}_K \cdot (\mathbf{B}\times\mathbf{J}_Q)] - \eta\nabla^2 \mathbf{B_K} \Big\}\, d\mathbf{x}^3. \tag{2.7}$$

Here, $E_U(K)$ and $E_B(K)$ denote the kinetic and magnetic energy in the shell K, respectively. The above equations can be written in the more compact form

$$\partial_t E_U(K) = \sum_Q [\mathscr{T}_{UU}(K,Q) + \mathscr{T}_{BU}(K,Q)] - \nu \mathscr{D}_U(K) + \mathscr{F}(K), \tag{2.8}$$

$$\partial_t E_B(K) = \sum_Q [\mathscr{T}_{UB}(K,Q) + \mathscr{T}_{BB}(K,Q)] - \eta \mathscr{D}_B(K). \tag{2.9}$$

The functions $\mathscr{T}_{UU}(K,Q)$, $\mathscr{T}_{UB}(K,Q)$, $\mathscr{T}_{BB}(K,Q)$, and $\mathscr{T}_{BU}(K,Q)$ express the energy transfer between different fields and shells,

$$\mathscr{T}_{UU}(K,Q) \equiv -\int \mathbf{U}_K (\mathbf{U}\cdot\nabla)\mathbf{U}_Q \, d\mathbf{x}^3, \tag{2.10}$$

$$\mathscr{T}_{UB}(K,Q) \equiv \int \mathbf{U}_K (\mathbf{B}\cdot\nabla)\mathbf{B}_Q \, d\mathbf{x}^3, \tag{2.11}$$

$$\mathscr{T}_{BU}(K,Q) \equiv \int \mathbf{B}_K (\mathbf{B}\cdot\nabla)\mathbf{U}_Q \, d\mathbf{x}^3. \tag{2.12}$$

In general, for positive transfer, the first subindex denotes the field that receives energy, the second subindex the field that gives energy. The first wavenumber corresponds to the field receiving energy, and the second wavenumber to the field giving energy. As an example, positive $\mathscr{T}_{UU}(K,Q)$ represents energy transferred from the velocity field at the shell Q to velocity field at the shell K. In the same way, positive $T_{UB}(K,Q)$ represents energy transferred from the magnetic field at wavenumbers Q to the velocity field at wavenumbers K.

The transfer of magnetic to magnetic energy $\mathscr{T}_{BB}(K,Q)$ in Hall MHDs consists of two terms

$$\mathscr{T}_{BB}(K,Q) = \mathscr{T}_{BB}^{\mathrm{MHD}}(K,Q) + \mathscr{T}_{BB}^{\mathrm{Hall}}(K,Q) \tag{2.13}$$

where

$$\mathscr{T}_{BB}^{\mathrm{MHD}}(K,Q) \equiv -\int \mathbf{B}_K (\mathbf{U}\cdot\nabla)\mathbf{B}_Q \, d\mathbf{x}^3, \tag{2.14}$$

is the usual MHD transfer of magnetic energy through advection by the bulk velocity field, and

$$\mathscr{T}_{BB}^{\mathrm{Hall}}(K,Q) \equiv \epsilon \int \mathbf{J}_K \cdot (\mathbf{B}\times\mathbf{J}_Q) \, d\mathbf{x}^3, \tag{2.15}$$

is the transfer of magnetic energy due to the Hall current. Note that the definition of the transfer terms corresponds to the MHD case in Alexakis et al. (2005b), except for the new term $\mathscr{T}_{BB}^{\mathrm{Hall}}(K,Q)$. However, as will be shown later, the behavior of the rest of the transfer terms in Hall MHDs will also be indirectly modified by the presence of the Hall effect.

All of these transfer functions satisfy the identity

$$\mathscr{T}_{vw}(K,Q) = -\mathscr{T}_{wv}(K,Q), \tag{2.16}$$

where v, w can be either U or B. This detailed conservation is what allows us to define the terms as transfers of energy between shells. Note that other groupings of the nonlinear terms in the Hall-MHD equations would not satisfy this symmetry condition.

In (2.8) and (2.9) we also have two dissipation functions and the energy injection rate

$$\nu \mathscr{D}_U(K) \equiv \nu \int |\nabla \mathbf{U}_K|^2 \, d\mathbf{x}^3, \tag{2.17}$$

$$\eta \mathscr{D}_B(K) \equiv \eta \int |\nabla \mathbf{B}_K|^2 \, d\mathbf{x}^3, \tag{2.18}$$

$$\mathscr{F}(K) \equiv \int \mathbf{f} \cdot \mathbf{U}_K \, d\mathbf{x}^3. \tag{2.19}$$

Finally, we can also define the transfer of magnetic helicity. From (2.2) we have

$$\partial_t H(K) = \sum_Q \mathscr{T}_H(K,Q) - \eta \mathscr{D}_H(K), \tag{2.20}$$

where the transfer of magnetic helicity from the wavenumber K to the wavenumber Q is given by

$$\mathscr{T}_H(K,Q) \equiv \int \mathbf{B}_K \cdot [(\mathbf{U} - \epsilon \mathbf{J}) \times \mathbf{B}_Q] \, d\mathbf{x}^3. \tag{2.21}$$

This transfer function satisfies the relation $\mathscr{T}_H(K,Q) = -\mathscr{T}_H(K,Q)$. The first term in (2.21) proportional to $\mathbf{U}$ is the usual transfer of H_M in MHD, while the second term proportional to $\epsilon \mathbf{J}$ is the contribution due to the Hall effect. Note that as a whole, magnetic helicity is transferred between the shells K and Q interacting with the electron velocity field $\mathbf{U} - \epsilon \mathbf{J}$. This is in agreement with the fact that in the ideal limit the magnetic field in the Hall-MHD system is frozen to the electron velocity field, instead of the bulk velocity field of the plasma as in MHDs.

The dissipation rate of magnetic helicity at the wavenumber K is given by

$$\eta \mathscr{D}_H(K) \equiv \eta \int \mathbf{B}_K \cdot \mathbf{J}_K \, d\mathbf{x}^3. \tag{2.22}$$

It is also worth noting that, since the magnetic helicity is not a positive defined quantity contrary to the energy, the interpretation of its transfer is more difficult. We will not attempt here a separation of its different sign components (see, e.g. Waleffe (1991) and Chen et al. (2003a,b) for the case of kinetic helicity in hydrodynamic turbulence).

The functions $\mathscr{D}_U$, $\mathscr{D}_B$, and $\mathscr{D}_H$ do not couple fields at different scales. As a result these functions can damp the amplitude of the transfer functions $\mathscr{T}$ as smaller scales are reached, but cannot give a transfer of energy or magnetic helicity between different scales.

3. Transport coefficients

In Mininni et al. (2002), the expression of the α dynamo coefficient was derived for Hall MHDs. Although an expression of the Hall-MHD turbulent diffusivity was derived by Mininni et al. (2003b), the closure was only valid for specific solutions of the Hall-MHD equations. To interpret the results from the energy transfer, it will be useful to have expressions for all the turbulent transport coefficients in the

induction equation. To this end, and for the sake of simplicity, we will use mean field theory (MFT) (Steenbeck et al. 1966; Krause and Raedler 1980) and the reduced smooth approximation (RSA) (Blackman and Field 1999). RSA was introduced to solve some ambiguities present in MFT when the magnetic field is strong enough to affect the velocity field through the Lorentz force. Although there are still assumptions in MFT not completely justified, at least a qualitative agreement has been observed with simulations in the MHD case (Brandenburg 2001) and the Hall-MHD case (Mininni et al. 2003a, 2005b). The transport coefficients can also be derived using more elaborate closures, such as the Lagrangian history direct interaction approximation (LHDIA) or the eddy damped quasi normal Markovian (EDQNM) closures (see, e.g. Lesieur 1997). It is worth noting that the analysis that follows in Secs 4 and 5 is of general validity and independent of the assumptions we will use here to derive the turbulent transport coefficients.

We split the fields into

$$\mathbf{U} = \bar{\mathbf{U}} + \mathbf{u} + \mathbf{u}_0, \tag{3.1}$$

$$\mathbf{B} = \bar{\mathbf{B}} + \mathbf{b} + \mathbf{b}_0, \tag{3.2}$$

where $\mathbf{u}_0$ and $\mathbf{b}_0$ are isotropic and homogeneous solutions of (2.1) and (2.5) in the absence of the mean fields $\bar{\mathbf{U}}$ and $\bar{\mathbf{B}}$. The fields with overbars are large-scale fields, and $\mathbf{u}$ and $\mathbf{b}$ are small-scale corrections to the isotropic and homogeneous solutions due to the presence of the large-scale fields. The fluctuating fields satisfy $\langle \mathbf{u} \rangle = \langle \mathbf{u}_0 \rangle = \langle \mathbf{b} \rangle = \langle \mathbf{b}_0 \rangle = 0$, where the brackets denote an average that satisfies Taylor's hypothesis (Krause and Raedler 1980). Replacing in (2.5), using the equations for the $\mathbf{u}_0$ and $\mathbf{b}_0$ fields, dropping terms quadratic in the fluctuating fields $\mathbf{u}$ and $\mathbf{b}$, and averaging leads to

$$\partial_t \bar{\mathbf{B}} = \nabla \times [(\bar{\mathbf{U}} - \epsilon \bar{\mathbf{J}}) \times \bar{\mathbf{B}} + \varepsilon] + \eta \nabla^2 \bar{\mathbf{B}}, \tag{3.3}$$

where ε is the mean field electromotive force

$$\varepsilon = \langle \mathbf{u}_0^{\mathrm{e}} \times \mathbf{b} + \mathbf{u}^{\mathrm{e}} \times \mathbf{b}_0 \rangle. \tag{3.4}$$

Our main aim in this section is to close (3.3) and write ε only as a function of averages of the fields $\mathbf{u}_0$, $\mathbf{b}_0$, and spatial derivatives of $\bar{\mathbf{B}}$. A simple argument of symmetry shows that in the approximately isotropic case

$$\varepsilon = \alpha \bar{\mathbf{B}} - \beta \nabla \times \bar{\mathbf{B}} + \gamma \nabla \times \nabla \times \bar{\mathbf{B}}. \tag{3.5}$$

From (2.1) and (2.5), and subtracting the equations for the mean flows, we can also write equations for the evolution of the turbulent fluctuations $\mathbf{u}$ and $\mathbf{b}$. We drop terms quadratic in $\mathbf{u}$ and $\mathbf{b}$, and keep only terms to zeroth and linear order in $\bar{\mathbf{B}}$,

$$\partial_t \mathbf{b} = \nabla \times (\bar{\mathbf{U}} \times \mathbf{b}_0 + \mathbf{u}_0^{\mathrm{e}} \times \bar{\mathbf{B}} + \epsilon \mathbf{b}_0^{\mathrm{e}} \times \bar{\mathbf{J}} + \mathbf{u}^{\mathrm{e}} \times \mathbf{b}_0 + \mathbf{u}_0^{\mathrm{e}} \times \mathbf{b} - \varepsilon) + \eta \nabla^2 \mathbf{b}. \tag{3.6}$$

In this equation, ε involves averaged quantities, and from the Taylor's hypothesis it gives no contribution to the mean electromotive force. The fourth and fifth terms on the right-hand side can be dropped using RSA, namely that $|\mathbf{u}|, |\mathbf{b}| \ll |\bar{\mathbf{B}}|$ (note that this condition is less stringent than the usual assumptions in MFT, since the amplitude of the fields $\mathbf{u}_0$, $\mathbf{b}_0$ can be much larger than the amplitude of the mean magnetic field). We will assume that the viscosity and diffusivity are small, and as a result we will also drop the last term on the right-hand side of (3.6). Terms proportional to $\bar{\mathbf{U}}$ can be removed in the proper frame of reference. Finally, we

obtain

$$\partial_t \mathbf{b} \approx \nabla \times (\mathbf{u}_0^{\mathrm{e}} \times \bar{\mathbf{B}} + \epsilon \mathbf{b}_0^{\mathrm{e}} \times \bar{\mathbf{J}}). \tag{3.7}$$

The second term on the right-hand side of (3.7) involves only spatial derivatives of $\bar{\mathbf{B}}$ and gives no contribution to the α coefficient, but is retained here since it will give contributions to β and γ.

Following the same steps, we can also write an equation for the evolution of $\mathbf{u}$,

$$\partial_t \mathbf{u} \approx \bar{\mathbf{B}} \cdot \nabla \mathbf{b}_0 + \mathbf{b}_0 \cdot \nabla \bar{\mathbf{B}} - \nabla p. \tag{3.8}$$

To obtain the mean field electromotive force we replace time derivatives in (3.6) and (3.8) by the inverse of a correlation time τ. This step, common in MFT, assumes the existence of a finite correlation time. At present there is no evidence of its validity in general (see, e.g. Gruzinov and Diamond 1995; Blackman and Field 2002; Brandenburg and Subramanian 2005). Since we are introducing a correlation time to close these equations, the expressions obtained for the turbulent transport coefficients will be considered as symbolic expressions.

Before replacing the expression for $\mathbf{u}$ in (3.5), (3.8) has to be solved for the small-scale pressure p. We will use a technique developed by Gruzinov and Diamond (1995) (see also Blackman and Field 2002). The α effect is linear in $\bar{\mathbf{B}}$ and therefore the correct result can be obtained assuming $\bar{\mathbf{B}}$ is uniform. Then $\partial_t \mathbf{u} \approx \bar{\mathbf{B}} \cdot \nabla \mathbf{b}_0$. Replacing the time derivative by τ^{-1} and replacing the expression in (3.5), we obtain in the weak isotropic case

$$\alpha = \frac{\tau}{3} \langle -\mathbf{u}_0^{\mathrm{e}} \cdot \nabla \times \mathbf{u}_0^{\mathrm{e}} + \mathbf{b}_0 \cdot \nabla \times \mathbf{b}_0 - \epsilon \mathbf{b}_0 \cdot \nabla \times \nabla \times \mathbf{u}_0^{\mathrm{e}} \rangle. \tag{3.9}$$

To compute β and γ we have to keep spatial derivatives of $\bar{\mathbf{B}}$ in (3.8), and therefore we have to solve for the pressure. This was done by Gruzinov and Diamond (1995) transforming (3.8) to Fourier space, and doing a Taylor expansion of the projector operator for incompressible $\mathbf{u}$ assuming a large-scale separation between the mean and fluctuating fields. In three spatial dimensions, it was shown that the pressure and $\mathbf{b}_0 \cdot \nabla \bar{\mathbf{B}}$ terms give no contribution to ε in (3.4). As a result, we are only left with the terms proportional to spatial derivatives of $\bar{\mathbf{B}}$ when (3.7) and the first term on the right-hand side of (3.8) are replaced on (3.4). Again, assuming weak isotropy, we obtain the expressions for the remaining turbulent transport coefficients

$$\beta = \frac{\tau}{3} \langle {\mathbf{u}_0^{\mathrm{e}}}^2 + \epsilon (\mathbf{u}_0 \cdot \nabla \times \mathbf{b}_0^{\mathrm{e}} + \mathbf{b}_0 \cdot \nabla \times \mathbf{u}_0^{\mathrm{e}}) \rangle, \tag{3.10}$$

$$\gamma = -\frac{\tau \epsilon}{3} \langle \mathbf{b}_0 \cdot \mathbf{u}_0^{\mathrm{e}} \rangle. \tag{3.11}$$

The two last terms in α and the third term in β come from the small-scale momentum equation and are related with the backreaction of the magnetic field into the velocity field. In the kinematic regime of a dynamo, $\alpha = -\tau/3 \langle \mathbf{u}_0^{\mathrm{e}} \cdot \nabla \times \mathbf{u}_0^{\mathrm{e}} \rangle$, which for $\epsilon = 0$ reduces to the MHD case (Krause and Raedler 1980). The general expression for $\epsilon = 0$ reduces to the MHD expression first found using the EDQNM closure by Pouquet et al. (1976), $\alpha = \tau/3 \langle -\mathbf{u}_0^{\mathrm{e}} \cdot \nabla \times \mathbf{u}_0^{\mathrm{e}} + \mathbf{b}_0 \cdot \nabla \times \mathbf{b}_0 \rangle$. Note also that in the MHD case in three dimensions, the turbulent diffusivity $\beta = -\tau \langle {\mathbf{u}_0}^2 \rangle / 3$ is not changed during the nonlinear saturation (Gruzinov and Diamond 1995).

The turbulent diffusivity β in Hall MHDs is not positive definite, in contrast to the pure MHD case (note that negative effective diffusivities can be found in MHDs if the assumption of homogeneity is dropped; see, e.g. Lanotte et al. (1999)). A negative value of β represents non-local transfer of energy from the small-scale

turbulent fields to the large-scale magnetic field. This result will be of interest in the following sections.

It is worth studying the values of β for particular cases. If ϵ is large enough and the system is magnetically dominated ($E_B \gg E_U$), then $\beta \approx -\tau\epsilon^2\langle j_0^2\rangle/3$, where $\mathbf{j}_0 = \nabla\times\mathbf{b}_0$ and we assumed that the average is a spatial average. In this case, β is always negative implying transfer of energy from the small scales to the large.

The normal modes of the Hall-MHD equations are circular polarized ($\nabla\times\mathbf{u}_0^{\rm e} = \pm k\mathbf{u}_0^{\rm e}$, $\nabla\times\mathbf{b}_0 = \pm k\mathbf{b}_0$) and dispersive, and in the limit $k \gg 1$ they satisfy dispersion relations $\omega \sim \epsilon k^2\bar{B}$ (whistlers, right-handed polarized) and $\omega \sim \bar{B}/\epsilon$ (ion-cyclotron waves, left-handed polarized). Also, for these waves the fields are related by $\mathbf{b}_0 = -k\bar{B}/\omega\mathbf{u}_0^{\rm e}$ (Mahajan et al. 2005a). If we assume a background of waves, $\beta \sim \tau/3\langle {u_0^{\rm e}}^2\rangle(1 \pm 2\epsilon k^2\bar{B}/\omega)$, which for k large enough can give positive or negative turbulent diffusivity according to the orientation of the wave. Note that from the dispersion relations, at small scales whistlers give a finite contribution to the turbulent diffusivity, while ion-cyclotron waves give a much larger turbulent diffusivity that grows as k^2.

4. Simulations

In this section we summarize the simulations that will be used to compute the energy and helicity transfer functions defined in Sec. 2. We performed three simulations in three dimensions with periodic boundary conditions, using a pseudospectral Hall-MHD code as described in Mininni et al. (2003a, 2005b). Runge–Kutta of second order is used to evolve the system of (2.1) and (2.2). To ensure the divergence-free condition for the magnetic field, a curl is removed from (2.2) and the equation for the vector potential is instead solved, with the Couloumb's gauge $\nabla\cdot\mathbf{A} = 0$. The three simulations are done with a spatial resolution of $N^3 = 256^3$ grid points. The $\frac{2}{3}$ dealiasing rule is used, and as a result the maximum wavenumber resolved by the code is $k_{\rm max} = N/3 \approx 85$. The kinematic viscosity and magnetic diffusivity are set to $\nu = \eta = 2\times10^{-3}$, and all of the simulations are well resolved, in the sense that the kinetic [$k_\nu = (\langle\omega^2\rangle/\nu^2)^{1/4}$] and magnetic [$k_\eta = (\langle J^2\rangle/\eta^2)^{1/4}$] dissipation wavenumbers are smaller than $k_{\rm max}$ at all times.

In Hall MHDs, the Courant–Friedrichs–Levy (CFL) condition is more stringent than for MHDs for which, with equipartition of kinetic and magnetic energy, the CFL condition for explicit time-stepping imposes an upper boundary on the time step $\Delta t \lesssim \Delta x/U_{\rm A}$ where Δx is the spatial step. In Hall MHDs, the dispersive nature of the whistlers impose $\Delta t \lesssim \Delta x^2/(\epsilon U_{\rm A})$. As a result, smaller time steps will be needed as ϵ is increased. Also, since the time step decreases quadratically as the spatial resolution is linearly increased, we cannot achieve spatial resolutions higher than 256^3 because of these constraints.

A helical forcing at $k_0 = 2$ given by an ABC flow

$$\mathbf{f} = [C\sin(k_0 z) + B\cos(k_0 y)]\hat{x} + [A\sin(k_0 x) + C\cos(k_0 z)]\hat{y} + [B\sin(k_0 y) + A\cos(k_0 x)]\hat{z}, \tag{4.1}$$

with $A = 0.9$, $B = 1$, and $C = 1.1$ was applied in the momentum equation. This election of the amplitude coefficients was done to ensure breaking of the symmetries of the ABC flow and ensuring a faster development of turbulence (Archontis et al. 2003). After a first hydrodynamic run made to reach a turbulent steady state, a

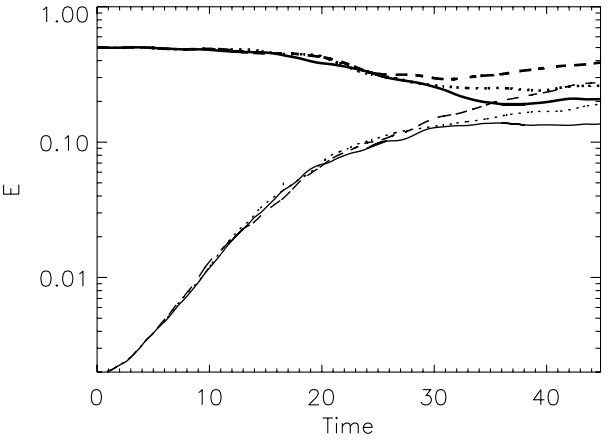

Figure 1. Kinetic (thick curves) and magnetic energy (thin curves) as a function of time, for runs with $\epsilon = 0$ (solid lines), $\epsilon = 0.05$ (dotted lines), and $\epsilon = 0.1$ (dashed lines).

random and small magnetic field was introduced at small scales. Initially the ratio of kinetic to magnetic energy was $E_u/E_b \sim 10^{-3}$.

The simulation was continued to see exponential growth of the magnetic energy (in the following, we will refer to this stage as the kinematic regime), and finally nonlinear saturation of the small-scale magnetic field (in the following, Hall-MHD turbulence). Three simulations were done, with $\epsilon = 0$ (MHD), $\epsilon = 0.05$ (which corresponds to $k_{\rm Hall} \approx 20$), and $\epsilon = 0.1$ ($k_{\rm Hall} \approx 10$). Figure 1 shows the time history of the kinetic and magnetic energies for these three runs.

After $t \approx 20$, the small-scale magnetic fields have reached saturation for all values of ϵ, while the large-scale magnetic field keeps growing slowly. As ϵ is increased, the magnetic energy reached by the system after the nonlinear saturation of the small scales increases. However, this behavior is not monotonical in ϵ as shown by Mininni et al. (2003a).

The saturation of the large-scale magnetic field takes place in a longer time (Brandenburg 2001; Mininni et al. 2005b). Note that one of the biggest challenges for DNS is to attain scale separation between the different dynamical ranges that must be resolved. Reynolds numbers in simulations are much smaller than the values observed in astrophysics and geophysics. Moreover, compared with hydrodynamics and MHDs, the extra characteristic length scale in Hall MHDs (the Hall scale) makes it even harder to achieve a proper separation between all of these scales. As a result, we will focus in this work on the energy transfer at scales smaller than k_0 (the energy injection band), and the late time large-scale evolution of these runs will not be discussed here (more details can be found, e.g. in Mininni et al. (2005b)).

Figure 2 shows the time evolution of the magnetic and kinetic energy spectra, for the runs with $\epsilon = 0.05$ and 0.1. As previously mentioned ($t \approx 40$) the spectrum of energy at scales smaller than k_0 has saturated and reached a steady state, while the magnetic energy at $k = 1$ keeps growing slowly. Note that the ratio of kinetic to magnetic energy at small scales in the saturated state depends on the value of ϵ. The Kolmogorov power spectrum is also shown as a reference in Fig. 2. Ideally, a large separation between the forcing and dissipation scales would be required in the simulation to have a clear inertial range. As noted before, the CFL-whistler condition makes simulations at higher resolutions and Reynolds numbers very

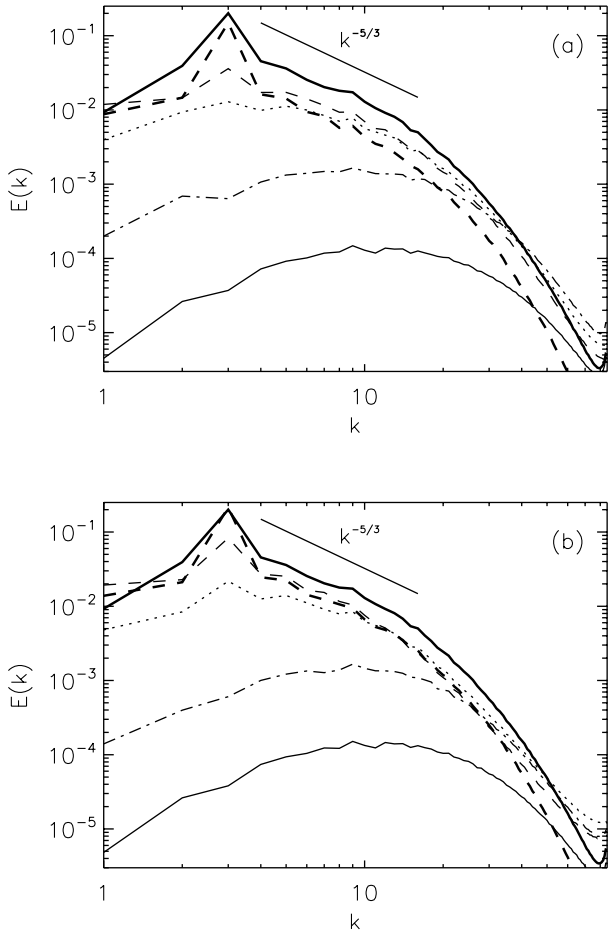

Figure 2. Spectra of kinetic energy (thick curves) and magnetic energy (thin curves) as a function of time, for $t = 5$ (solid), 15 (dash-dotted), 30 (dotted), and 45 (dashed): (a) $\epsilon = 0.05$ and (b) $\epsilon = 0.1$. The Kolmogorov scaling is shown as a reference.

expensive. However, it is worth noting here that in the study of energy transfer in hydrodynamic and MHD turbulence (Alexakis et al. 2005a,b) no qualitative differences were observed as the Reynolds number and the resolution were increased. With these results in mind, we will study the energy and helicity transfer in Hall MHDs in 256^3 simulations.

Another quantity that will be of interest in the next section is the magnetic helicity. Figure 3 shows the time history of the absolute value of magnetic helicity for the three runs. Note that while in the MHD run ($\epsilon = 0$) the magnetic helicity grows monotonically with time, in the Hall-MHD runs the time evolution is strongly modified. For $\epsilon = 0.05$ the magnetic helicity grows slower than in the MHD case, and for $\epsilon = 0.1$ it changes sign at $t \approx 24$. As was observed by Mininni et al. (2003a), the Hall effect inhibits the generation of net magnetic helicity at large scales by the helical dynamo process. This inhibition grows monotonically with the amplitude of Hall term, and for values of ϵ large enough the magnetic helicity fluctuates around zero. The reason for this behavior will be discussed in the next section.

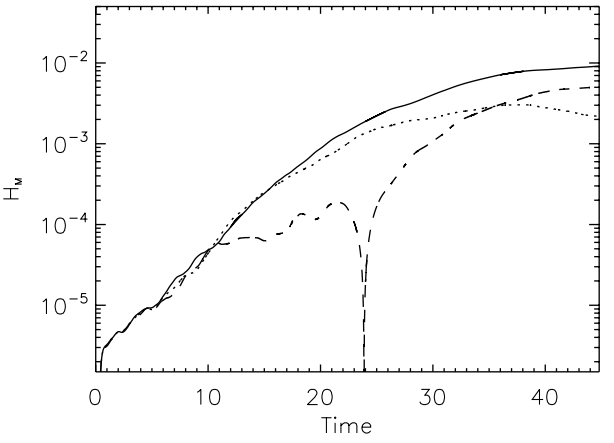

Figure 3. Absolute value of the magnetic helicity as a function of time. Curves are as in Fig. 1. For $\epsilon = 0.1$ the magnetic helicity changes sign from negative to positive at $t \approx 24$.

5. Transfers

In this section we discuss the energy transfer terms defined in Sec. 2 as obtained from the three DNSs discussed in the previous section.

5.1. The run with $\epsilon = 0.1$

We start discussing in detail the transfer in the Hall-MHD run with $\epsilon = 0.1$. At late times in this simulation, when the system is close to equipartition ($U_A \approx U$), the Hall wavenumber is $k_{\rm Hall} \approx 10$. Since we consider transfer functions at different times, for the sake of comparison and unless explicitly said, all transfers in this section will be normalized using the root mean square velocity and magnetic field according to their expressions (2.10)–(2.15). Note that since $\epsilon\mathbf{J}$ has units of velocity (and $\mathbf{U} - \epsilon\mathbf{J}$ is the electron velocity), the transfer function $T_{BB}^{\rm Hall}$ is normalized using $\langle B^2|\mathbf{U}|\rangle$. This election also allows for a direct comparison of this term against $T_{BB}^{\rm MHD}$ (see (2.14)).

Figure 4 shows the transfer of kinetic energy from the shell $Q = 20$ to kinetic energy in shells K for three different times. As previously mentioned, positive transfer denotes energy given by the shell Q, while negative transfer corresponds to energy received by this shell. In this case, kinetic energy in the shell $Q = 20$ is mostly received from the shell $K = 18$ (negative peak), and given to $K = 22$ (positive peak). This function represents the local and direct transfer of kinetic energy to small scales. There are no noticeable differences in this transfer between the Hall-MHD runs ($\epsilon = 0.05$ and 0.1) and the MHD run ($\epsilon = 0$).

The curve for early times (kinematic regime) corresponds to the initial exponential growth of magnetic energy, and is a time average properly normalized. As time evolves and the magnetic energy grows, the amount of kinetic energy transferred to small scales diminishes, since a larger amount of kinetic energy at large scales is turned into magnetic energy. This effect was previously observed in MHD runs (Mininni et al. 2005a).

The inset in Fig. 4 shows the $T_{UU}(K, Q)$ transfer at late times for $Q = 5$, 10, 15, and 20. Although as we move to larger wavenumbers Q the amplitude of the transfer is slightly damped because of dissipation, the overall shape of the transfer function is not modified. As a result, and since in this run $k_{\rm Hall} \approx 10$, we will continue the

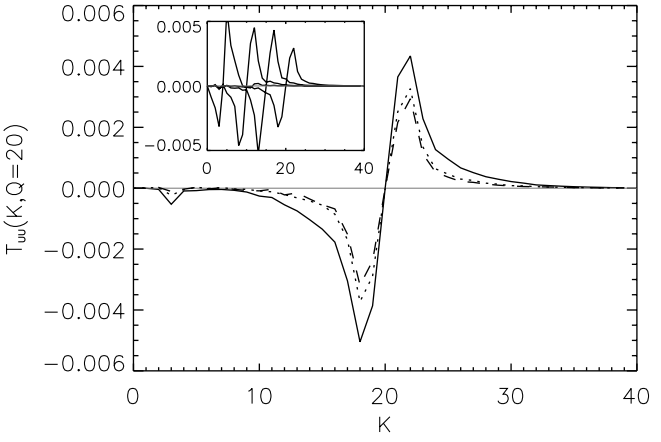

Figure 4. Transfer of kinetic energy from $Q = 20$ to K, $\mathscr{T}_{UU}(K, Q = 20)$, in the kinematic regime (solid curve), at $t = 26$ (dotted curve), and at $t = 45$ (dashed curve) in the run with $\epsilon = 0.1$. The inset shows $\mathscr{T}_{UU}(K, Q)$ in the same run at $t = 45$ for $Q = 5$, 10, 15, and 20.

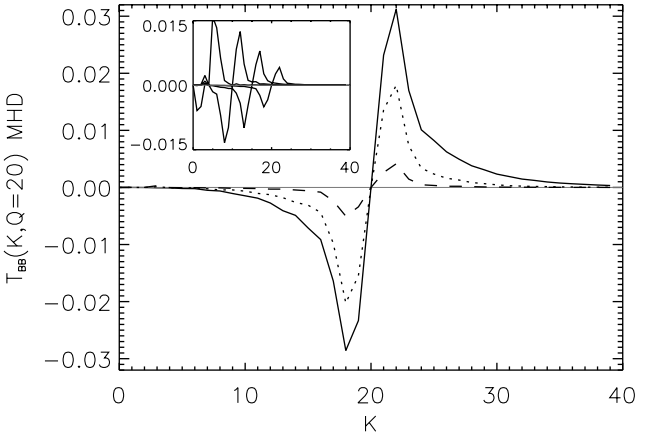

Figure 5. $\mathscr{T}^{\rm MHD}_{BB}(K, Q = 20)$ in the kinematic regime (solid curve), at $t = 26$ (dotted curve), and at $t = 45$ (dashed curve) in the run with $\epsilon = 0.1$. The inset shows $\mathscr{T}^{\rm MHD}_{BB}(K, Q)$ in the same run at $t = 45$ for $Q = 5$, 10, 15, and 20.

analysis for $Q = 20$ and show results for different values of Q for comparison when required.

Figure 5 shows $\mathscr{T}^{\rm MHD}_{BB}(K, Q = 20)$, the transfer of magnetic energy at the shell $Q = 20$ to magnetic energy in shells K due to the advection by the bulk velocity field. As in the case of $\mathscr{T}_{UU}$, the transfer is local and the shell $Q = 20$ receives most of the energy from $K = 18$ (negative peak) and gives energy to the shell $K = 22$ (positive peak). Again, no significant differences are observed between the three runs with different values of ϵ, except that this transfer, in amplitude, gets substantially stronger as ϵ (and **B**) increases.

The total shell-to-shell transfer of magnetic energy is given by $\mathscr{T}^{\rm MHD}_{BB}$ plus $\mathscr{T}^{\rm Hall}_{BB}$. Figure 6 shows the $\mathscr{T}^{\rm Hall}_{BB}(K, Q)$ transfer at $Q = 20$. As in the previous cases, positive transfer denotes energy is given from the shell $Q = 20$ to shells K, while negative transfer indicates the shell Q receives energy from K. The $\mathscr{T}^{\rm Hall}_{BB}$ transfer

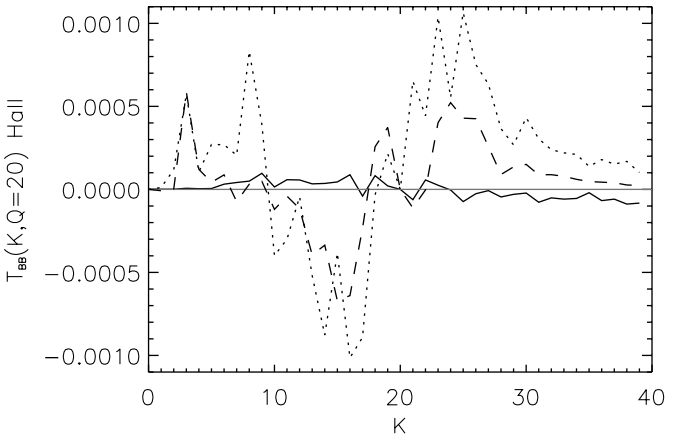

Figure 6. $\mathscr{T}_{BB}^{\rm Hall}(K, Q = 20)$ in the kinematic regime (solid curve), at $t = 26$ (dotted curve), and at $t = 45$ (dashed curve) in the run with $\epsilon = 0.1$.

is small during the kinematic regime, but grows as the small scales reach nonlinear saturation. Although this transfer is noisier than the previous terms studied, two regions can be identified at late times. Around $Q = K = 20$, the transfer is local and direct: positive and negative peaks can be observed at $K \approx 25$ and $K \approx 15$, indicating energy is received and given, respectively, by the shell Q from and to these wavenumbers. On the other hand, at large scales (up to $K \approx 10$) a region with positive transfer can also be identified. This region indicates a non-local and inverse transfer of energy: the shells with K between 1 and 10 receive magnetic energy from the shell $Q = 20$. This combination of a local direct transfer of energy and a non-local inverse transfer is characteristic of the Hall term, and is in qualitative agreement with the turbulent dissipation derived in Sec. 3 where it was shown that it can take negative values.

The remaining transfer term is $\mathscr{T}_{BU}(K, Q)$, which when positive represents transfer of kinetic energy from the shell Q to magnetic energy in the shell K. Although the expression of this transfer function is equal for MHDs and Hall MHDs, the transfer is modified by the Hall currents. The reason for this can be explained in two ways. On the one hand, the expression of the α-effect in Sec. 3 is modified by the Hall term, and this term represents transfer of energy from the turbulent velocity field to the mean magnetic field. On the other hand, waves are expected to give non-local coupling between the velocity and magnetic fields (see, e.g. Iroshnikov 1963; Kraichnan 1965) in MHDs. In Hall MHDs, the non-dispersive Alfvén waves of MHDs are replaced by dispersive circularly polarized waves and, as a result, the coupling between the two fields should also be modified.

Figure 7 shows $\mathscr{T}_{BU}(K = 20, Q)$, the energy transferred to the magnetic field at $K = 20$ from the velocity field at shells Q. In the kinematic regime this transfer is non-local and similar to the MHD transfer (Alexakis et al. 2005b; Mininni et al. 2005a): the magnetic field at $K = 20$ receives energy from the large-scale flow at $Q = 3$ and from all turbulent scales up to $Q \approx 20$. However, at late times the transfer is strongly modified. The magnetic field at $K = 20$ still receives energy from a broad range of wavenumbers Q smaller than K (as was found in Alexakis et al. 2005b), but it also receives energy from larger wavenumbers ($Q \approx 22$) and gives energy to the velocity field at slightly smaller wavenumbers ($Q \approx 18$). Note that

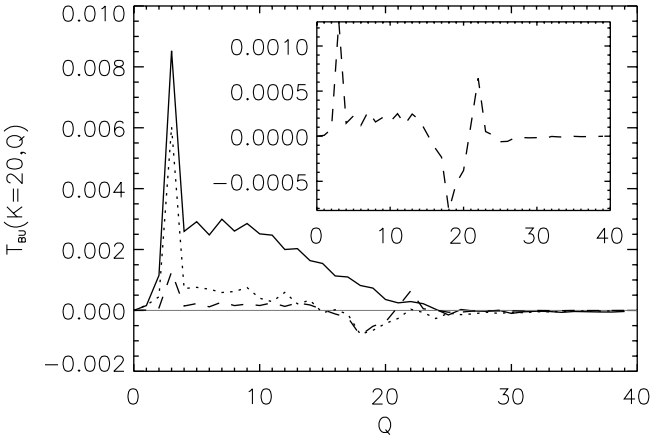

Figure 7. $\mathscr{T}_{BU}(K = 20, Q)$ in the kinematic regime (solid curve), at $t = 26$ (dotted curve), and at $t = 45$ (dashed curve) in the run with $\epsilon = 0.1$. The inset shows a blow up of the last transfer.

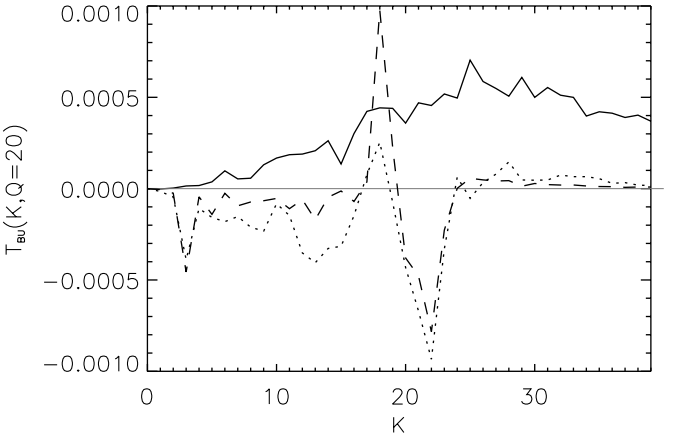

Figure 8. $\mathscr{T}_{BU}(K, Q = 20)$ at three different times: the kinematic regime (solid curve), $t = 26$ (dotted curve), and $t = 45$ (dashed curve) for the run with $\epsilon = 0.1$.

this indicates that in Hall MHDs a magnetic field at a given scale can give rise to velocity fluctuations at larger scales, a process studied by Mahajan et al. (2005b) and referred to there as the *reverse dynamo*.

Figure 8 shows $\mathscr{T}_{BU}(K, Q = 20)$, the energy received by the magnetic field at all wavenumbers K from the velocity field in the shell $Q = 20$. During the kinematic regime, the velocity field in this shell gives energy to all magnetic shells, although the transfer peaks at wavenumbers larger than Q. However, in the saturated regime, the transfer changes drastically again. The magnetic field at wavenumbers K smaller than $Q \approx 16$, and in shells between 20 and 23 gives energy to the velocity field (negative transfer), while the magnetic field in shells between $K \approx 16$–20 and for $K \gtrsim 23$ receives energy from the velocity field (positive transfer). This is just the counterpart of $\mathscr{T}_{BU}(K, Q)$ for constant K, and again shows that in Hall MHDs a small-scale magnetic field can create large-scale flows.

Figure 9 shows shaded plots of $\mathscr{T}_{BB}^{\rm Hall}(K, Q)$ and $\mathscr{T}_{BU}(K, Q)$ at different times. These are the two transfers that are strongly modified by the Hall currents, and the

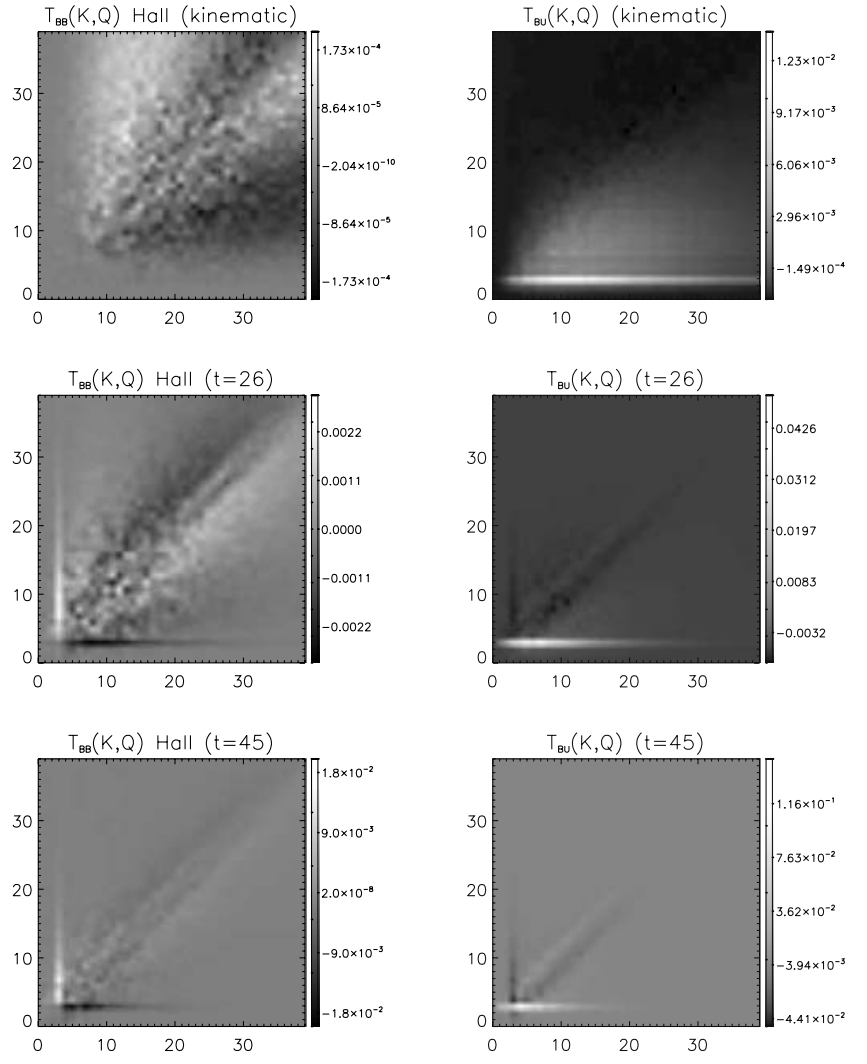

Figure 9. $\mathscr{T}^{\rm Hall}_{BB}(K,Q)$ (left column), and $\mathscr{T}_{BU}(K,Q)$ (right column) at three different times: the kinematic regime (top), $t = 26$ (middle), and $t = 45$ (bottom) for the run with $\epsilon = 0.1$. In all figures, K is on the x-axis and Q on the y-axis. Shading goes from dark ($\mathscr{T} < 0$) to light ($\mathscr{T} > 0$).

figures allow for a study of the terms for all values of K and Q. Although noisy, a characteristic pattern can be recognized in $\mathscr{T}^{\rm Hall}_{BB}$. As time evolves and the magnetic energy grows, the relative importance of this term grows. For wavenumbers $K, Q \gtrsim k_{\rm Hall} \sim 10$, the function is positive (light) near and below the diagonal $K = Q$, and negative (dark) near and above this diagonal. This region close to the diagonal represents local and direct transfer of energy: a cut at constant Q shows that close to the diagonal the shell Q receives energy from neighboring shells with $K \lesssim Q$ (negative $\mathscr{T}^{\rm Hall}_{BB}$) and gives energy to neighbor shells with $K \gtrsim Q$ (positive $\mathscr{T}^{\rm Hall}_{BB}$). As we move far from this diagonal, the sign of the regions above and below the diagonal changes. This indicates a non-local and inverse transfer of magnetic energy, from

small to large scales, in agreement with the expression for the turbulent magnetic diffusivity obtained in Sec. 3.

The $\mathscr{T}_{BU}(K,Q)$ also shows an interesting behavior as a function of time. During the kinematic regime, $\mathscr{T}_{BU}$ is positive in a triangle defined by $K \gtrsim Q$. This indicates that the velocity field in a given shell amplifies the magnetic field in that shell and all of the shells with larger wavenumber (smaller scales). A strong band around $Q = 3$ is also observed, indicating that the velocity field in the energy injection band gives a lot of energy to the magnetic field. These results are similar to the kinematic MHD dynamo (see Mininni et al. 2005a). However, at late times an inverse process can be identified close to the diagonal $K = Q$. Above it, $\mathscr{T}_{BU}$ is positive, while below it, it is negative. This represents transfer of magnetic energy from a shell K to kinetic energy in slightly smaller wavenumbers Q.

Since $\mathscr{T}_{BB}^{\rm Hall}$ and $\mathscr{T}_{BU}$ give both direct and inverse transfers of energy (locally or non-locally), it is of interest to quantify which direction wins when all of the contributions to the transfer are added. To this end, we computed the contribution of each transfer term to the energy flux. The total energy flux at a wavenumber k is given by

$$\Pi(k) = \sum_{K=0}^{k} \sum_{Q} \mathscr{T}(K,Q), \tag{5.1}$$

where $\mathscr{T} = \mathscr{T}_{UU} + \mathscr{T}_{BB} + \mathscr{T}_{UB} + \mathscr{T}_{BU}$ is the total energy transfer. We can split this flux into the energy flux due solely to the transfer of kinetic energy

$$\Pi_{UU}(k) = \sum_{K=0}^{k} \sum_{Q} \mathscr{T}_{UU}(K,Q), \tag{5.2}$$

the flux due to the transfer of magnetic energy $\Pi_{BB} = \Pi_{BB}^{\rm MHD} + \Pi_{BB}^{\rm Hall}$, where

$$\Pi_{BB}^{\rm MHD}(k) = \sum_{K=0}^{k} \sum_{Q} \mathscr{T}_{BB}^{\rm MHD}(K,Q), \tag{5.3}$$

$$\Pi_{BB}^{\rm Hall}(k) = \sum_{K=0}^{k} \sum_{Q} \mathscr{T}_{BB}^{\rm Hall}(K,Q), \tag{5.4}$$

and the hybrid flux due to interactions between the velocity and magnetic fields

$$\Pi_{BU}(k) = \sum_{K=0}^{k} \sum_{Q} [\mathscr{T}_{BU}(K,Q) + \mathscr{T}_{UB}(K,Q)]. \tag{5.5}$$

To compute the fluxes, the transfer functions are not normalized.

Figure 10 shows the partial energy fluxes at $t = 45$. Since all transfer functions were computed up to $K, Q = 40$, the partial fluxes go to zero artificially at this wavenumber, although in the simulation the total energy flux goes to zero only at the maximum resolved wavenumber $k_{\rm max}$.

The total flux is positive at wavenumbers larger than k_0 (the energy injection band), indicating a direct cascade of the total energy. At wavenumbers smaller than k_0 the total flux is negative, evidence of large-scale dynamo action. A substantial portion of the total flux is due to the transfer of energy from the kinetic to the magnetic reservoirs (Π_{BU}), and this contribution to the flux is positive at

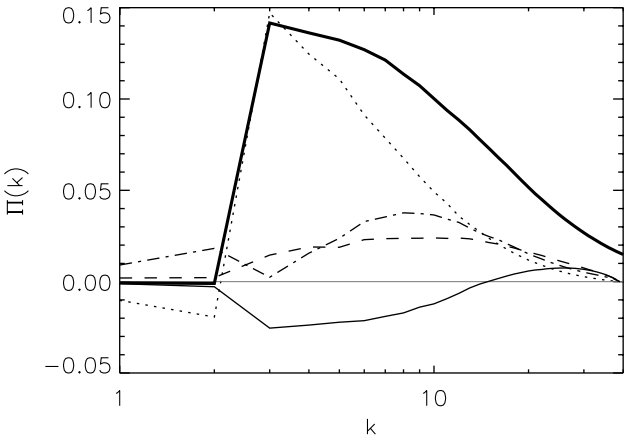

Figure 10. Energy fluxes in the run with $\epsilon = 0.1$ at $t = 45$: $\Pi_{BB}^{\rm Hall}(k)$ (solid curve), $\Pi_{BB}^{\rm MHD}(k)$ (dash-dotted curve), $\Pi_{UU}(k)$ (dashed curve), and $\Pi_{BU}(k)$ (dotted curve). The thick curve is the total flux in the simulation.

all wavenumbers (larger than the forced ones) indicating a net direct transfer of the energy. We note that this flux is due to the non-local T_{UB} and T_{BU} transfer terms. The flux due to the transfer of kinetic energy Π_{UU} is also positive at all wavenumbers. However, the flux due to the transfer of magnetic energy $\Pi_{BB}^{\rm Hall}$ is only positive at wavenumbers larger than $k_{\rm Hall}$. For wavenumbers smaller than $k \approx 10 \sim k_{\rm Hall}$, $\Pi_{BB}^{\rm Hall}$ changes sign, giving as a result a net inverse transfer of magnetic energy, from small to large scales. This indicates that a magnetically dominated Hall-MHD system could display backscatter of the magnetic energy. Magnetic fluctuations at small scales could give rise to large-scale magnetic fields, as is also implied by the expression of β found in Sec. 3.

Note that although in MHDs the inverse cascade of magnetic helicity can give a similar result, the backscatter predicted in Hall MHDs by the turbulent diffusivity is novel, since it can take place even in the absence of helicity in the fields. To illustrate this we show results of non-helical magnetically dominated simulations in Sec. 6. It is worth noting that at wavenumbers smaller than $k_{\rm Hall}$, the Hall term increases the flux of magnetic energy to smaller scales, thus also in agreement with results showing the Hall currents increase the amount of small-scale perturbations (Birn et al. 2001; Laveder et al. 2002a,b; Morales et al. 2005).

5.2. Dependence with ϵ

Now we discuss in detail the dependence of the results as ϵ (or the Hall scale) is varied. To this end, we consider the runs with $\epsilon = 0.1$, 0.05, and 0 (MHD). As previously mentioned, the transfer terms $\mathscr{T}_{UU}(K,Q)$ and $\mathscr{T}_{BB}(K,Q)$ do not show a dependence with the amplitude of the Hall effect. These terms give direct and local transfer of energy to small scales, as in MHDs (Alexakis et al. 2005b). As a result, we will discuss the change in the remaining transfer terms as ϵ is varied.

Since the Hall effect is more relevant when the magnetic field is stronger, we will consider the transfer terms at $t = 45$, when a large-scale magnetic field is present and the small scales have reached saturation. Since we will examine runs with different values of ϵ at the same time, in this section the transfers are not normalized using the energies.

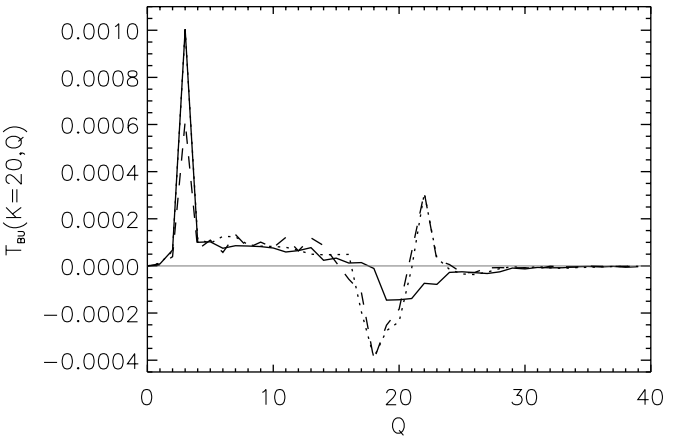

Figure 11. $\mathscr{T}_{BU}(K=20,Q)$ at $t=45$ for $\epsilon=0$ (solid curve), 0.05 (dotted curve), and 0.1 (dashed curve).

The transfer of magnetic energy due to the Hall term $\mathscr{T}_{BB}^{\rm Hall}(K,Q=20)$ is of course zero in the MHD case ($\epsilon=0$). As ϵ is increased, except for an increase in its amplitude (not shown), no significant differences are observed and its behavior is similar to that examined in Sec. 5.

Figure 11 shows the behavior of $\mathscr{T}_{BU}(K=20,Q)$ (the transfer of kinetic energy in the shells Q to magnetic energy in the shell $K=20$) as ϵ is varied. The strong peak at $Q=3$ is associated with the injection band. This transfer is non-local in the three runs, as is evidenced by the positive plateau from $Q\approx 3$ to $Q\approx 16$. As a result, the velocity field in all of these shells gives energy to the magnetic field at $K=20$. As ϵ is increased, a local transfer grows in the neighborhood of $Q=20$. The velocity field at wavenumbers K slightly larger give energy to the magnetic field at $K=20$, while the magnetic field gives energy to the velocity field at wavenumbers slightly smaller ($Q\approx 18$).

We can compute the energy flux as ϵ increases. Since the transfer of kinetic energy is not changed, we will focus on two contributions to the total flux: the flux of magnetic energy $\Pi_{BB}(k)$, and the hybrid flux $\Pi_{BU}(k)$ due to the terms turning kinetic into magnetic energy and *vice versa*. The magnetic energy flux $\Pi_{BB}=\Pi_{BB}^{\rm MHD}+\Pi_{BB}^{\rm Hall}$ is shown in Fig. 12. At scales larger than $k_{\rm Hall}$, negative flux of magnetic energy is observed, giving backscatter of magnetic energy to large scales. As ϵ is increased, the amplitude of the backscatter grows, and the wavenumber where the flux changes sign moves to larger k.

Figure 13 shows the flux $\Pi_{BU}(k)$. At wavenumbers smaller than the forcing wavenumber ($k=3$), the flux is negative. This is a signature of large-scale dynamo action: the magnetic field at large scales is fed by the small-scale velocity field. Remarkably, as ϵ is increased, the amplitude of the negative flux at large scales increases. This is in good agreement with dynamo simulations where the large-scale magnetic field was observed to grow faster in the presence of Hall currents (Mininni et al. 2003a, 2005b).

5.3. Transfer of magnetic helicity

We discuss briefly the transfer of magnetic helicity in the saturated case $t=45$. To study the transfer associated with the inverse cascade of magnetic helicity at

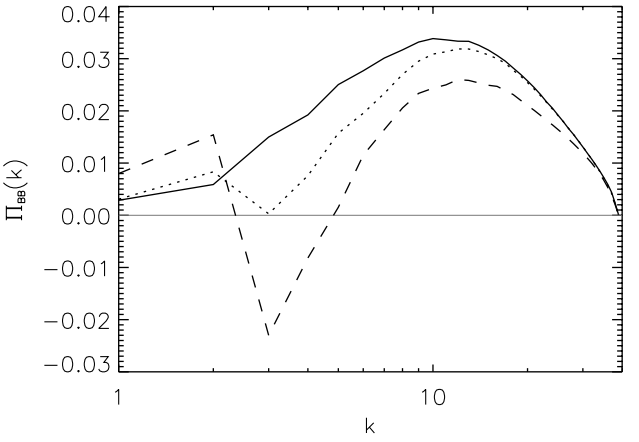

Figure 12. $\Pi_{BB}(k)$ at $t = 45$ for $\epsilon = 0$ (solid curve), 0.05 (dotted curve), and 0.1 (dashed curve).

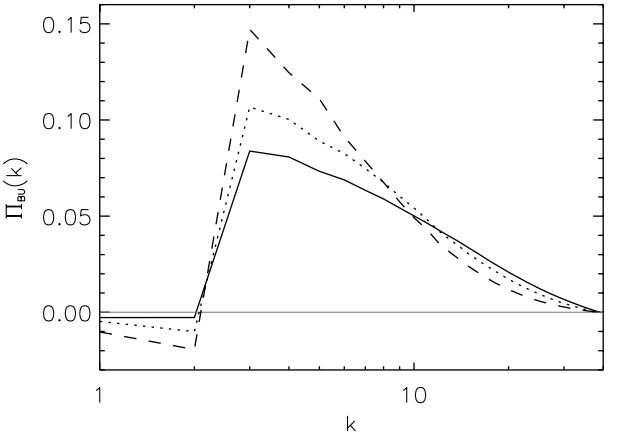

Figure 13. $\Pi_{BU}(k)$ at $t = 45$ for $\epsilon = 0$ (solid curve), 0.05 (dotted curve), and 0.1 (dashed curve).

scales larger than the forcing scale, a large separation between this scale and the largest scale in the box is needed. At a fixed spatial resolution, this reduces the Reynolds numbers, and as a result also reduces the separation between the Ohmic scale and the Hall scale. This study is beyond the aim of this work. However, we want to point out a remarkable feature observed in the transfer of magnetic helicity at scales smaller than the forcing scale.

Figure 14 shows the transfer $\mathscr{T}_H(K, Q = 20)$ normalized by the magnetic helicity in the shell $Q = 20$ at $t = 45$. The transfer is mostly local in the three simulations, peaking at wavenumbers K slightly smaller and larger than Q. However, as ϵ is increased the transfer rate of magnetic helicity is strongly quenched. This slow down in the transfer in Hall MHDs explains the behavior observed in Fig. 3. In MHD and Hall-MHD dynamos, the external mechanical forcing generates equal amounts of magnetic helicity of opposite sign at scales smaller and larger than the forcing band (Seehafer 1996; Brandenburg 2001; Mininni et al. 2003a). Since the transfer of magnetic helicity between different shells in the Hall-MHD runs

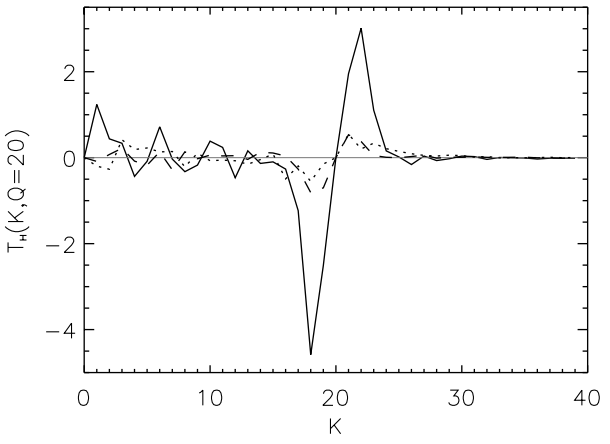

Figure 14. $\mathscr{T}_H(K, Q = 20)$ normalized by the magnetic helicity at the shell $Q = 20$, at $t = 45$ for $\epsilon = 0$ (solid curve), 0.05 (dotted curve), and 0.1 (dashed curve).

is almost stopped, it takes more time for the magnetic helicity at scales smaller than the forcing scale to reach the dissipative scale where it can be destroyed. As a result, both signs of magnetic helicity pile up close to the forcing band, decreasing the growth rate of net magnetic helicity at scales larger than the forcing scale, and also allowing for the possibility for a sign change of the net magnetic helicity.

6. Backscatter of magnetic energy in Hall MHDs

The mechanically forced runs discussed in the previous section show negative flux of magnetic energy at large scales due to the Hall effect, in agreement with negative values of the turbulent diffusivity. This indicates that in a magnetically dominated simulation, backscatter of magnetic energy could be observed if the Hall term is strong enough. Note that here we are using the word *backscatter* to refer to this transfer of magnetic energy from the small to the large scales. This is done in opposition to the usual terminology of inverse cascades, since we have been unable to identify any ideal invariant of the Hall-MHD equations cascading inversely with constant flux to the large scales.

To study this scenario, we performed three simulations with $\epsilon = 0$, 0.2, and 0.5. The kinematic viscosity and magnetic diffusivity were $\nu = \eta = 3.5 \times 10^{-2}$, and the spatial resolution was $N^3 = 128^3$. The initial condition was $\mathbf{U} = \mathbf{B} = 0$. The system was forced with a non-helical and random electromotive force given by a superposition of harmonic modes at wavenumbers $k = 9$ and 10. The phases of the force were changed with a correlation time of $\tau = 1.25 \times 10^{-2}$, and the time step was set to $\Delta t = 1.5 \times 10^{-3}$. Note that in the absence of magnetic helicity, no inverse cascade is expected in the MHD case (see, however, Lanotte et al. (1999) for cases where a large-scale shear is present).

The system was run until reaching a turbulent steady state. All of the quadratic invariants (with the exception of the total energy) were verified to be small: the magnetic helicity fluctuates in the three runs around zero, both the global quantity as well as its spectral density at each individual Fourier shell. Figure 15 shows the kinetic and magnetic energy spectrum at early times ($t = 3$). The shell of

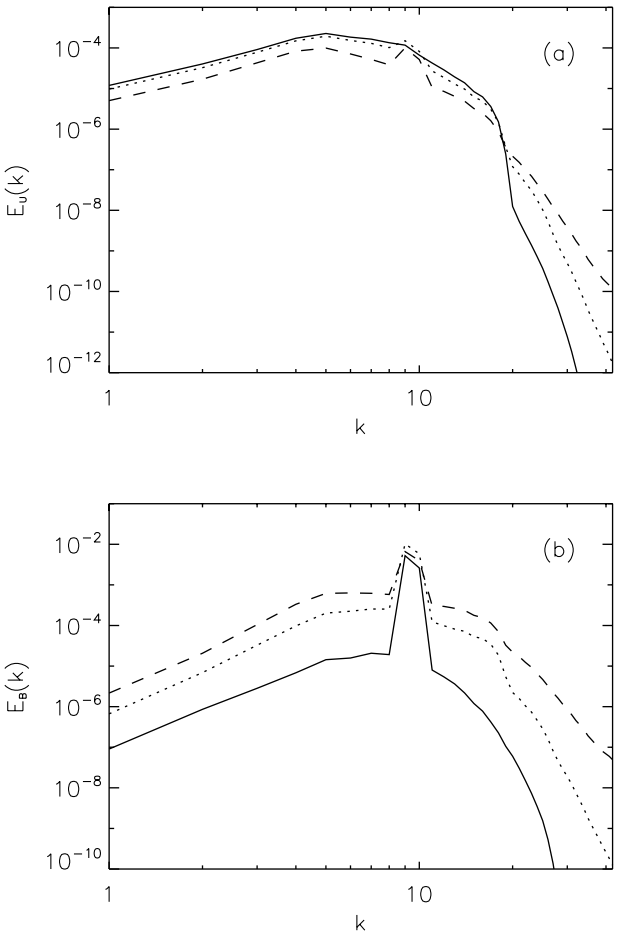

Figure 15. (a) Kinetic energy spectrum $E_U(k)$ and (b) magnetic energy spectrum $E_B(k)$ at $t = 3$, for runs with $\epsilon = 0$ (solid curve), 0.05 (dotted curve), and 0.1 (dashed curve).

wavenumbers associated with the external magnetic force is easily recognized in the peak in Fig. 15(b).

As time evolves, an increase in the magnetic energy at wavenumbers smaller than the forcing wavenumber is observed. Figure 16 shows the kinetic and magnetic energy spectrum at $t = 75$, when the system has reached a steady state. The three runs are dominated by the magnetic energy (note that the peak in the magnetic energy spectrum around the forcing band gives the largest contribution to the energy). The spectrum of kinetic energy is similar for the three runs, and large-scale perturbations are observed because of the injection of kinetic energy by the Lorentz force. However, the magnetic energy spectrum is strongly modified as ϵ is increased. While the spectra of the three simulations peak in the energy injection band, the magnetic energy at $K = 1$ in the run with $\epsilon = 0.5$ is three orders of magnitude larger than in the MHD run. The magnetic energy in all wavenumbers smaller than the forcing wavenumbers increases as ϵ is increased.

The backscatter of magnetic energy is in good agreement with the negative flux Π_{BB} observed in the previous section, and the negative turbulent transport

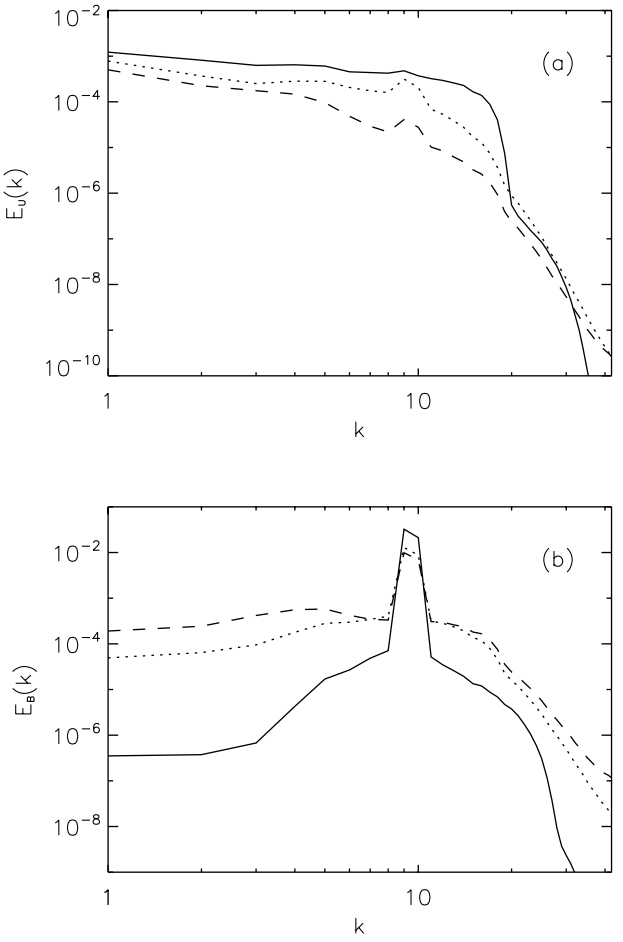

Figure 16. (a) Kinetic energy spectrum and (b) magnetic energy spectrum at $t = 75$ for runs with $\epsilon = 0$ (solid curve), 0.05 (dotted curve), and 0.1 (dashed curve).

coefficients derived for the magnetically dominated case. Note that an increase in the level of the small-scale magnetic fluctuations (for wavenumbers smaller than the energy injection wavenumbers) is also observed in Fig. 16(b).

7. Discussion

In this work we presented energy transfer in Hall-MHD turbulence as obtained from numerical simulations. The properties of the spectral transfer is one of the building blocks of turbulence theories, and to the best of our knowledge no attempt to study transfer and cascades of ideal invariants in this system of equations had been attempted before.

Before proceeding with the discussion of our results, we have to warn the reader about a clear limitation of the numerical results presented. As previously mentioned, an astrophysics-like scale separation between the box size, the energy injection scale, the Hall scale, and the Ohmic dissipation scale is well beyond today's computing resources. We tested the dependence of our results as ϵ was varied, but no

attempt was made to change the Reynolds numbers in our simulations. This being said, we believe that even under this limitation, an understanding of the transfer of energy between different scales is of utmost importance for the development of a theory of turbulence for Hall MHDs or other extensions of MHDs to take into account kinetic plasma effects.

Direct evidence of non-locality of the energy transfer was observed. While the total energy displays a direct cascade to small scales, in the individual transfer terms, both directions (toward small and large scales) were identified. Coupling between the magnetic and velocity fields is strongly modified by the Hall effect, and a local backscatter of energy from the magnetic field to the velocity field at slightly larger scales was observed. This behavior can be expected since the Hall term changes the nature of the non-dispersive MHD Alfvén waves, into dispersive and circularly polarized waves. As a result, the nonlinear coupling between the two fields is also changed.

Also a non-local backscatter of magnetic energy was observed at scales larger than the Hall scale. This backscatter was verified in non-helical magnetically forced simulations, where the amplitude of the magnetic field at scales larger than the forcing scale was observed to grow in the Hall-MHD simulations, but not in the MHD run. In some sense, the magnetic field in Hall MHDs being frozen in the ideal case to the electron velocity field, couples non-locally both small scales (the current) and large scales (the bulk velocity field).

All of these processes can be partially explained considering transport turbulent coefficients estimated from MFT. Unlike MHDs, the turbulent diffusivity in Hall MHDs is not positive definite. In particular, its expression shows that ion-cyclotron waves are more likely to produce large values of negative (backscatter) or positive (reconnection) turbulent diffusivity than the whistler mode.

The transfer of magnetic helicity at small scales was also observed to be quenched by the Hall effect. While the mechanisms generating magnetic helicity in the Hall MHD dynamo are the same as in MHDs (Mininni et al. 2003a), the transport of helicity is expected to be changed by the Hall currents (Ji 1999). As a result of the slow down in the transfer rate of magnetic helicity by the Hall effect, the late time evolution of the system is not characterized by a maximally helical large-scale magnetic field as in the MHD case (Pouquet et al. 1976; Meneguzzi et al. 1981; Brandenburg 2001).

The Hall term gives a direct transfer of magnetic energy at scales smaller than the Hall scale, and an inverse transfer at scales larger than the Hall scale. This finding sheds light into the conflicting results reported in the literature, where the Hall effect was observed to increase the amount of small scales and magnetic dissipation in some cases, and to help large-scale reorganization processes in other cases, as mentioned in the introduction.

As a result of this dual direction of the Hall transfer, a change in the power law followed by the total energy spectrum can be expected close to the Hall wavenumber. Steepening of the energy spectrum for wavenumbers smaller than $k_{\rm Hall}$ was observed in 2.5-dimensional simulations with strong magnetic fields imposed, when the cross-correlation between the velocity and magnetic fields was significant (Ghosh et al. 1996). In three-dimensional dynamo simulations where the cross-correlation is in general small, no change was observed (Mininni et al. 2005b), although a faster growth of the large-scale magnetic field was found. Given the non-local nature of the transfer in Hall MHDs, and the scale separation needed

to observe a clear change in the energy spectrum, probably a huge increase in the spatial resolution is needed to confirm it.

Acknowledgements

Computer time was provided by NCAR. The NSF grant CMG-0327888 at NCAR supported this work in part and is gratefully acknowledged.

References

Alexakis, A., Mininni, P. D. and Pouquet, A. 2005a *Phys. Rev. Lett.* **95**, 264503.

Alexakis, A., Mininni, P. D. and Pouquet, A. 2005b *Phys. Rev.* E **72**, 046301.

Archontis, V., Dorch, S. B. F. and Nordlund, A. 2003 *Astron. Astrophys.* **410**, 759.

Balbus, S. A. and Terquem, C. 2001 *Astrophys. J.* **552**, 235.

Bhattacharjee, A., Ma, Z. W. and Wang, X. 1999 *J. Geophys. Res.* **104**, 14543.

Birn, J., Drake, J. F., Shay, M. A., Rogers, B. N., Denton, R. E., Hesse, M., Kuznetsova, M., Ma, Z. W., Bhattacharjee, A., Otto, A. and Pritchett, P. L. 2001 *J. Geophys. Res.* **106**, 3715.

Blackman, E. G. and Field, G. B. 1999 *Astrophys. J.* **521**, 597.

Blackman, E. G. and Field, G. B. 2002 *Phys. Rev. Lett.* **89**, 265007.

Brandenburg, A. 2001 *Astrophys. J.* **550**, 824.

Brandenburg, A. and Subramanian, K. 2005 *Phys. Rep.* **417**, 1.

Chen, Q., Chen, S. and Eyink, G. L. 2003a *Phys. Fluids* **15**, 361.

Chen, Q., Chen, S., Eyink, G. L. and Holm, D. D. 2003b *Phys. Rev. Lett.* **90**, 214503.

Debliquy, O., Verma, M. K. and Carati, D. 2005 *Phys. Plasmas* **12**, 042309.

Ding, W. X., Brower, D. L., Craig, D., Deng, B. H., Fiksel, G., Mirnov, V., Prager, S. C., Sarff, J. S. and Svidzinski, V. 2004 *Phys. Rev. Lett.* **93**, 045002.

Domaradzki, J. A. and Rogallo, R. S. 1990 *Phys. Fluids* **2**, 413.

Galanti, B., Kleeorin, N. and Rogachevskii, I. 1995 *Phys. Plasmas* **2**, 4161.

Ghosh, S., Siregar, E., Roberts, D. A. and Goldstein, M. L. 1996 *J. Geophys. Res.* **101**, 2493.

Gruzinov, A. V. and Diamond, P. H. 1995 *Phys. Plasmas* **2**, 1941.

Helmis, G. 1968 *Mon. sber. Deutsch. Akad. Wiss. Berlin* **10**, 280.

Iroshnikov, P. S. 1963 *Sov. Astron.* **7**, 566.

Ji, H. 1999 *Phys. Rev. Lett.* **83**, 3198.

Kraichnan, R. H. 1965 *Phys. Fluids* **8**, 1385.

Krause, F. and Raedler, K.-H. 1980 *Mean-field Magnetohydrodynamics and Dynamo Theory*. New York: Pergamon.

Lanotte, A., Noullez, A., Vergassola, M. and Wirth, A. 1999 *Geophys. Astrophys. Fluid Dyn.* **91**, 131.

Laveder, D., Passot, T. and Sulem, P. L. 2002a *Phys. Plasmas* **9**, 293.

Laveder, D., Passot, T. and Sulem, P. L. 2002b *Phys. Plasmas* **9**, 305.

Lesieur, M. 1997 *Turbulence in Fluids*. Dordrecht: Kluwer Academic.

Mahajan, S. M., Mininni, P. D. and Gómez, D. O. 2005a *Astrophys. J.* **619**, 1014.

Mahajan, S. M., Shatasvili, N. L., Mikeladze, S. V. and Sigua, K. I. 2005b *Astrophys. J.* **634**, 419.

Mahajan, S. M. and Yoshida, Z. 1998 *Phys. Rev. Lett.* **81**, 4863.

Meneguzzi, M., Frisch, U. and Pouquet, A. 1981 *Phys. Rev. Lett.* **47**, 1060.

Mininni, P. D., Alexakis, A. and Pouquet, A. 2005a *Phys. Rev.* E **72**, 046302.

Mininni, P. D., Gómez, D. O. and Mahajan, S. M. 2002 *Astrophys. J.* **567**, L81.

Mininni, P. D., Gómez, D. O. and Mahajan, S. M. 2003a *Astrophys. J.* **587**, 472.

Mininni, P. D., Gómez, D. O. and Mahajan, S. M. 2003b *Astrophys. J.* **584**, 1120.

Mininni, P. D., Gómez, D. O. and Mahajan, S. M. 2005b *Astrophys. J.* **619**, 1019.
Mirnov, V. V., Hegna, C. C. and Prager, S. C. 2003 *Plasma Phys. Rep.* **29**, 566.
Morales, L., Dasso, S. and Gómez, D. 2005 *J. Geophys. Res.* **110**, A04204.
Numata, R., Yoshida, Z. and Hayashi, T. 2004 *Comp. Phys. Comm.* **164**, 291.
Ohkitani, K. and Kida, S. 1992 *Phys. Fluids* A **4**, 794.
Ohsaki, S. 2005 *Phys. Plasmas* **12**, 032306.
Pouquet, A., Frisch, U. and Léorat, J. 1976 *J. Fluid Mech.* **77**, 321.
Rezeau, L. and Belmont, G. 2001 *Space Sci. Rev.* **95**, 427.
Rheinhardt, M. and Geppert, U. 2002 *Phys. Rev. Lett.* **88**, 101103.
Sano, T. and Stone, J. M. 2002 *Astrophys. J.* **570**, 314.
Seehafer, N. 1996 *Phys. Rev.* E **53**, 1283.
Shay, M. A., Drake, J. F., Rogers, B. N. and Denton, R. E. 2001 *J. Geophys. Res.* **106**, 3759.
Smith, D., Ghosh, S., Dmitruk, P. and Matthaeus, W. H. 2004 *J. Geophys. Res.* **31**, L02805.
Steenbeck, M., Krause, F. and Rädler, K.-H. 1966 *Z. Naturforsch.* **21a**, 369.
Turner, L. 1986 *IEEE Trans. Plasma Sci.* **14**, 849.
Verma, M. 2004 *Phys. Rep.* **401**, 229.
Waleffe, F. 1991 *Phys. Fluids* A **4**, 350.
Wang, X., Bhattacharjee, A. and Ma, Z. W. 2001 *Phys. Rev. Lett.* **87**, 265003.
Yeung, P. K., Brasseur, J. and Wang, Q. 1995 *J. Fluid Mech.* **283**, 43.
Zeldovich, Y. B., Ruzmaikin, A. A. and Sokoloff, D. D. 1983 *Magnetic Fields in Astrophysics*. New York: Gordon and Breach.
Zhou, Y. 1993 *Phys. Fluids* A **5**, 2511.